Catalysis Today 150 (2010) 332–339

Contents lists available at ScienceDirect

Catalysis Today

journal homepage: www.elsevier.com/locate/cattod

Dependence of chemical composition of calcined hydrotalcite-like compounds for SO_x reduction

Manuel Sanchez-Cantu [a], Lydia M. Perez-Diaz [a], Ana M. Maubert [b], Jaime S. Valente [b,c,*]

[a] BUAP, Facultad de Ingeniería Química, Av. San Claudio y 18 Sur, CP 72570, Puebla, Mexico
[b] UAM–Azcapotzalco, Quimica de Materiales, Av. San Pablo # 180, CP 02200 Mexico, D.F., Mexico
[c] Instituto Mexicano del Petróleo, Eje Central # 152, CP 07730 Mexico, D.F., Mexico

ARTICLE INFO

Article history:
Available online 31 October 2009

Keywords:
Hydrotalcite-like compounds
Mixed oxides
SO_x reduction
FCC process

ABSTRACT

Binary and ternary hydrotalcite-like (HT) materials containing copper, nickel, zinc, iron, magnesium and/or aluminum were synthesized by coprecipitation and characterized by elemental analysis, powder X-ray diffraction and N_2 adsorption–desorption at −196 °C. Samples were calcined at 700 °C for 4 h, obtaining mixed oxides which were tested for sulfur oxides (SO_x) removal. Their performance was compared with a commercial SO_x reducing additive by thermogravimetric SO_x uptake. SO_x adsorption was carried out by contacting the calcined solid with a mixture of 1% SO_2 in air at 650 °C. The adsorbed species were reduced with H_2 at 550 °C, 650 °C and 700 °C, in order to study their stability and the solid's regenerability. It was found that the isomorphic incorporation of a transition metal in the HT layers increased the mixed oxide's reduction ability. This was reflected on higher reduction rates and sulfate reduction amounts at 550 °C. Furthermore, these materials showed greater adsorption–reduction properties than the commercial additive.

1. Introduction

In the last years, atmospheric pollution has become one of the main global concerns. Combustion of fossil fuels is still the main energy source, resulting in increasing toxic and greenhouse gases emissions. Amongst these emissions, sulfur oxides, a mixture of SO_2 + SO_3 commonly referred to as SO_x, are one of the most dangerous. They contribute directly to acid rain formation and to the destruction of the ozone layer. Most of the global emission of sulfur oxides comes from energy power plants (∼65%) and the fluid catalytic cracking (FCC) process in refinery plants (∼7%) [1].

Stringent environmental regulations limiting the atmospheric SO_x emissions encourage the research for more efficient ways to reduce them. Due to the strong acid character of SO_x, basic oxides such as MgO, Al_2O_3, etc., have been proposed to trap these molecules [2]. The method for SO_x removal must be closely related to the emission source. For instance, in power plants, fuels and/or coal are burned to produce energy; sulfur compounds, contained in the feedstock, are oxidized producing SO_x gases that are released to the atmosphere. In this sense, many strategies have been proposed to reduce these emissions, *e.g.*, by changing the operating conditions and using fuels with lower sulfur contents or natural gas. However, the most popular and less expensive method for SO_x emissions removal is the addition of selective sorbents to the fuel [3,4]. Compounds such as Al_2O_3, MgO, $MgCO_3$, CaO and $CaCO_3$, among others, have been tested as SO_x sorbents [5,6]. The main problem found with these sorbents is their SO_x adsorption velocity and capacity. Usually, only a small fraction of the sorbent reacts in the relatively short contact time.

In the FCC process, the SO_x production and removal mechanisms are different from those of energy power plants. For such purposes, the characteristics of the sorbent should be different. After cracking reactions, the catalyst is deactivated and the coke deposited on it is burnt, to regenerate the catalyst activity. During heating, the sulfur compounds present in coke are oxidized (>90% to SO_2 and <10% to SO_3), producing SO_x emissions in the regeneration zone by the following mechanism:

$$S_{coke} + O_2 \rightarrow SO_2 + SO_3 \quad (1)$$

In a first stage, an efficient sorbent (commonly known as additive since it is added in small amounts to the total catalyst inventory) must have the capacity to oxidize sulfur dioxide to sulfur trioxide, which then binds to the surface producing a metallic sulfate:

$$SO_2 + 1/2O_2 \rightarrow SO_3 \quad (2)$$

$$MO + SO_3 \rightarrow MSO_4 \quad (3)$$

* Corresponding author at: Instituto Mexicano del Petróleo, Eje Central # 152, CP 07730 Mexico, D.F., Mexico. Tel.: +52 55 9175 8444.
E-mail addresses: jsanchez@imp.mx, sanchezvalente@yahoo.com (J.S. Valente).

0920-5861/$ – see front matter © 2009 Elsevier B.V. All rights reserved.
doi:10.1016/j.cattod.2009.09.010

MO in Eq. (3) represents the additive. During the second stage, the additive and the cracking catalyst travel to the riser. Once in the riser, the metallic sulfate is reduced by hydrogen and other reducing gases to regenerate the metal oxide, producing hydrogen sulfide and/or metallic sulfide:

$$MSO_4 + 4H_2 \rightarrow MS + 4H_2O \quad (4)$$

$$MSO_4 + 4H_2 \rightarrow MO + H_2S + 3H_2O \quad (5)$$

Finally, the metal sulfide can be hydrolyzed by steam in the stripper to regenerate the additive:

$$MS + H_2O \rightarrow MO + H_2S \quad (6)$$

Therefore, potential SO_x additives must have the following characteristics: (i) oxidize SO_2 to SO_3, (ii) form a stable metal sulfate at regenerator conditions, (iii) be able to release easily the sulfate species to regenerate the activity of the sorbent and (iv) do not modify conversion and selectivity of FCC products.

Worldwide research groups have studied several materials for this end, *e.g.*, MgO, Al_2O_3 and MgAl spinels were evaluated as possible additives. However, their performance was limited, in view of the fact that MgO forms a very stable $MgSO_4$, restricting the additive regeneration; besides, it has a low apparent bulk density and a low attrition index. Al_2O_3 showed a low SO_x removal capacity because the $Al_2(SO_4)_3$ formed is very unstable at the regenerator temperature (>700 °C) so it releases the sulfate species as produced in the regenerator. Eventually, $MgAl_2O_4$ spinels were also tested, but they showed low SO_x removal capacity and low sulfate reduction, which causes the solid's deactivation [7–11].

The use of cerium oxide as oxidation catalysts has been reported, more specifically as a promoter for the oxidation of SO_2 to SO_3 in the de-SO_x process from FCC units [12–16]. Indeed, cerium oxide has proved to be an excellent oxidation catalyst, and its success derives from its redox character. CeO_2 promotes SO_2 to SO_3 oxidation, by the following mechanism [17]:

$$2CeO_2 + SO_2 \rightarrow SO_3 + Ce_2O_3 \quad (7)$$

$$Ce_2O_3 + 1/2O_2 \rightarrow 2CeO_2 \quad (8)$$

The SO_3, being more reactive than SO_2, is rapidly adsorbed on the additive's basic sites as sulfates.

Cerium oxide is not used as a single phase, mainly because it is expensive compared with other materials used as SO_x reducing additives. For this reason, the use of iron spinels were proposed instead of cerium; iron has the ability to play a dual role, as oxidizing and reducing catalyst. Even so, studies on iron-containing systems showed that iron could be an undesirable constituent of an SO_x removal additive, in particular for coke formation, since the important role of coke in the overall thermal balance of FCC process is well known. However, it has been mentioned that this effect can be minimized or even eliminated by controlling the iron content in the material [18]. Notwithstanding, for a process where coke formation does not matter, for instance, in power plant process, the use of iron as an oxidation catalyst in SO_x removal processes represents an economically viable route.

In recent years, basic mixed oxides obtained from calcined hydrotalcite-like (HT) compounds have shown good SO_x and NO_x reduction activities, indicating their possible use as catalysts to reduce those emissions from several sources [3,4,19–21]. The structure of HTs resembles that of brucite, $Mg(OH)_2$, in which magnesium is octahedrally surrounded by hydroxyls. An HT structure is created by replacing some of the M^{2+} divalent cations for M^{3+} trivalent cations, turning the layered array positively charged. These positively charged M^{2+}–M^{3+} double hydroxide layers are electrically compensated for by anions, which are located in the interlayer region. A wide variety of synthetic hydrotalcite-like materials can be prepared, and they are represented by the general formula: $[M_{(1-x)}^{2+}M_x^{3+}(OH)_2]^{x+}[A^{n-}]_{x/n}\cdot mH_2O$, where $M^{2+} = Mg^{2+}$, Ni^{2+}, Zn^{2+}, etc.; $M^{3+} = Al^{3+}$, Fe^{3+}, Ga^{3+}, etc.; $A^{n-} = (CO_3)^{2-}$, Cl^-, $(NO_3)^-$, etc.

It has been reported that the physicochemical properties of the hydrotalcite-like compounds and the solid solutions produced after their calcination can be easily tuned by changing the nature and amount of metal cations and anions [22].

Therefore, to elucidate the role of the chemical composition on the catalytic SO_x removal performance, a series of bimetallic (MgAl, MgFe, NiAl and ZnAl) and trimetallic (MgFeAl, MgCuAl, MgNiAl, MgZnAl) hydrotalcite-like compounds were prepared. The calcined HTs were tested in a thermogravimetric SO_x uptake system and compared with a commercial SO_x reducing additive.

2. Experimental

Bimetallic (MgAl, MgFe, NiAl and ZnAl) and trimetallic ($MgM^{p+}Al$ where M^{p+} is Fe^{3+}, Ni^{2+}, Zn^{2+} and Cu^{2+}) hydrotalcite-like materials were prepared by coprecipitation following the procedure described elsewhere [23]. The general synthesis is as follows.

An aqueous solution containing the nitrates of the metallic salts (solution A) was prepared maintaining a M^{2+}/M^{3+} molar ratio of 3 and a transition metal content of 7%. An aqueous solution containing KOH and/or K_2CO_3 (solution B) was prepared by separate. Solutions A and B were added drop wise simultaneously into a glass reactor, at room temperature, maintaining the slurry's final pH between 8 and 10, depending on the solids chemical composition. The slurry was aged under vigorous stirring at 60 °C for 18 h; except for MgCuAl, which was aged for 30 min. The precipitate was washed several times and dried at 100 °C overnight. The dried samples are referred to in the text as fresh samples, in order to distinguish them from the calcined ones. The solids were labeled according to their chemical composition.

2.1. Characterization of solids

Solids' chemical composition was determined by X-ray fluorescence in a Siemens SRS 3000 X-ray spectrophotometer. Powder XRD patterns were recorded in a Siemens D-500 diffractometer, using Cu Kα radiation (λ = 1.5418 Å) in the 4–70° of the 2θ angle range. Textural analyses were performed by adsorption–desorption of nitrogen at −196 °C on an Autosorb-I apparatus. Prior to the analysis, the samples were calcined at 700 °C and outgassed in a vacuum (10^{-5} Torr) at 400 °C for 5 h. The surface areas were calculated by the Brunauer–Emmett–Teller (BET) method, and the pore size distribution and total pore volume were determined by the Brunauer–Joyner–Hallenda (BJH) method.

2.2. SO_x adsorption–reduction test

Thermogravimetric analyses were carried out using Perkin-Elmer TG-7. First, 50 mg of hydrotalcite-like compound were annealed at 700 °C in air for 4 h. Then the solid was reactivated at 650 °C to eliminate the species adsorbed during handling. SO_2 adsorption was carried out by contacting the solid with a mixture of 1% SO_2 in air. After reaching saturation, the system is flushed with nitrogen and then reduced with H_2 at 550, 650 and/or 700 °C, depending on the sample's requirements. To disclose the solid reusability, a new adsorption cycle was done. The performance of these materials was compared with a commercial SO_x additive.

Table 1
Chemical composition of the hydrotalcite-like compounds.

Sample	Chemical composition	M^{2+}/M^{3+}
MgAl	$[Mg_{0.744}Al_{0.256}(OH)_2](CO_3)_{0.128}{\cdot}0.850H_2O$	2.9
MgFe	$[Mg_{0.688}Fe_{0.311}(OH)_2](CO_3)_{0.160}{\cdot}0.800H_2O$	2.2
NiAl	$[Ni_{0.704}Al_{0.296}(OH)_2](CO_3)_{0.148}{\cdot}0.942H_2O$	2.4
ZnAl	$[Zn_{0.75}Al_{0.25}(OH)_2](CO_3)_{0.125}{\cdot}0.840H_2O$	3.0
MgCuAl	$[Mg_{0.658}Cu_{0.098}Al_{0.244}(OH)_2](CO_3)_{0.122}{\cdot}0.687H_2O$	3.1
MgNiAl	$[Mg_{0.547}Ni_{0.120}Al_{0.333}(OH)_2](CO_3)_{0.166}{\cdot}0.933H_2O$	2.0
MgFeAl	$[Mg_{0.714}Fe_{0.107}Al_{0.179}(OH)_2](CO_3)_{0.143}{\cdot}0.828H_2O$	2.5
MgZnAl	$[Mg_{0.493}Zn_{0.165}Al_{0.342}(OH)_2](CO_3)_{0.171}{\cdot}0.978H_2O$	1.9

3. Results and discussion

3.1. Physicochemical characterization

The chemical composition of the samples is reported in Table 1. Even though a nominal molar ratio M^{2+}/M^{3+} of 3 was established in all samples, the real M^{2+}/M^{3+} ratio varied from 1.9 for MgZnAl to 3.1 for MgCuAl, which is attributed to an incomplete incorporation of the cations inside the brucite-like layers. Nonetheless, it is worth noting, that the metal content does not depend on this molar ratio variation, since the desired metals are present in the layers, as is expressed by the formulas reported in Table 1.

Fig. 1 presents the X-ray diffraction pattern of the fresh samples. All of them exhibit the characteristic reflections of the pure hydrotalcite-like structure (JCPDS card 89-0460); no additional reflections suggesting the formation of secondary crystalline phases were detected. Unit cell parameters were obtained assuming a 3R stacking sequence; therefore, $a = 2d_{1\,1\,0}$ and $c = 3d_{0\,0\,3}$. The interlayer distance, $d_{0\,0\,3}$, is regulated by the water content together with the amount, size, orientation, and charge of the anion located between the brucite-like layers; and $d_{1\,1\,0}$ is the average cation–cation distance inside the brucite-like layers [24]. Crystal sizes were calculated from the Scherrer equation $L = 0.9\lambda/\beta\cos\theta$, where L is the crystallite size, λ the X-ray wavelength, β the line broadening and θ the Bragg angle [25]. The results are reported in Table 2.

It is well known [23,26,27] that, in order to obtain pure hydrotalcite-like phases, the molar ratio M^{2+}/M^{3+} is limited to 2–4. When the isomorphic substitution of a M^{2+} or a M^{3+} cation is performed, the cell parameter a may increase or decrease, and this variance will depend mainly on the ionic radii of the cations in octahedral coordination, which decreases in the following order: $Zn^{2+} > Cu^{2+} > Mg^{2+} > Ni^{2+} > Fe^{3+} > Al^{3+}$. Thus, a simple way to confirm the isomorphic substitution of divalent and/or trivalent cations is by analyzing the variation of the cell parameter a.

As can be seen in Table 2 the a values varied from 3.056 to 3.079 Å for MgAl and ZnAl, respectively; also the variation between MgAl and MgFe can be explained by the cation size differences, since the ionic radius of Fe^{3+} is bigger than that of Al^{3+}, 0.690 and 0.675 Å, respectively. The same effect of the ionic radius is displayed by the trimetallic HTs, if we compare MgAl against the MgNiAl and MgCuAl samples (a = 3.056, 3.041 and 3.058 Å, respectively).

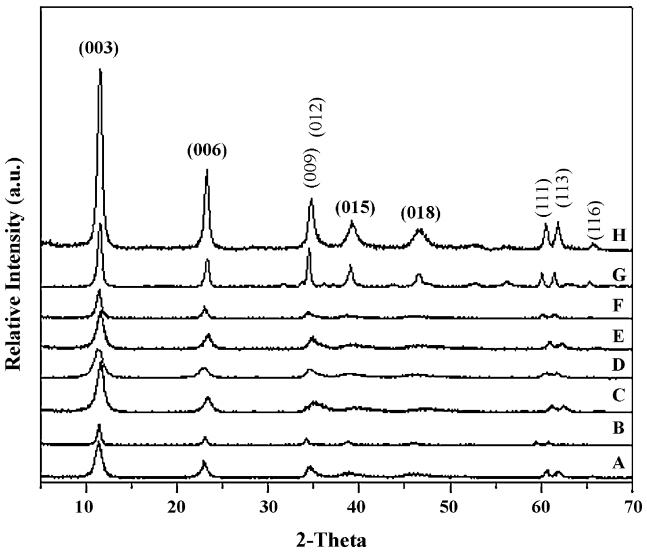

Fig. 1. X-ray powder patterns of fresh samples (A) MgAl, (B) MgFe, (C) NiAl, (D) ZnAl, (E) MgCuAl, (F) MgNiAl, (G) MgFeAl, and (H) MgZnAl.

The differences in c parameters between the various HT compounds can be attributed to the different coulombic attractive forces between the positively charged brucite-like layers and the anions located in the interlayer region [23,26,27]. As the cations' electronegativity increases, electrostatic interactions are stronger, thus reducing the interlayer distance. The electronegativity of the cations increases in the following order: Mg < Al < Zn < Ni∼Fe < Cu. Then, for instance, the c value of MgAl will be larger than that of NiAl (see Table 2). Regarding crystal size, all samples afford crystals that grew preferentially in the (1 1 0) rather than the (0 0 3) direction, see Table 2. In fact, MgFe, ZnAl and MgZnAl have bigger crystals; while the copper and nickel-containing samples (NiAl, MgNiAl, MgCuAl) have the smallest crystals. This fact is probably due to the Jahn–Teller distortion, in which the octahedral coordination of the metal (nickel or copper) is distorted such that the two axial bonds are either shorter than or longer than the other four bonds; this may have a hindering effect on crystallization process.

The specific surface area, pore volume, and average pore size of the solids calcined at 700 °C are reported in Table 2. All solids display high surface areas. The surface areas of the bimetallic compounds ranged from 48 to 204 m^2/g for ZnAl and MgAl,

Table 2
Cell parameters, crystal sizes and textural properties of the hydrotalcite-like compounds.

Sample	a (Å)	c (Å)	$L_{0\,0\,3}$ (Å)	$L_{1\,1\,0}$ (Å)	SSA[a] ($m^2\,g^{-1}$)	PV[b] ($cm^3\,g^{-1}$)	Pore diameter (Å)	
							I	II
MgAl	3.056	23.310	106	212	204	0.847	43	389
MgFe	3.106	23.128	250	442	75	0.696	28	378
NiAl	3.029	22.822	92	133	186	0.543	33	114
ZnAl	3.079	22.964	221	261	48	0.394	36	811
MgCuAl	3.058	23.289	72	101	183	0.337	37	87
MgNiAl	3.041	22.868	102	152	251	0.603	29	90
MgFeAl	3.073	23.194	153	191	169	0.558	30	164
MgZnAl	3.047	22.671	125	236	193	0.870	29	189

[a] Specific surface area.
[b] Pore volume.

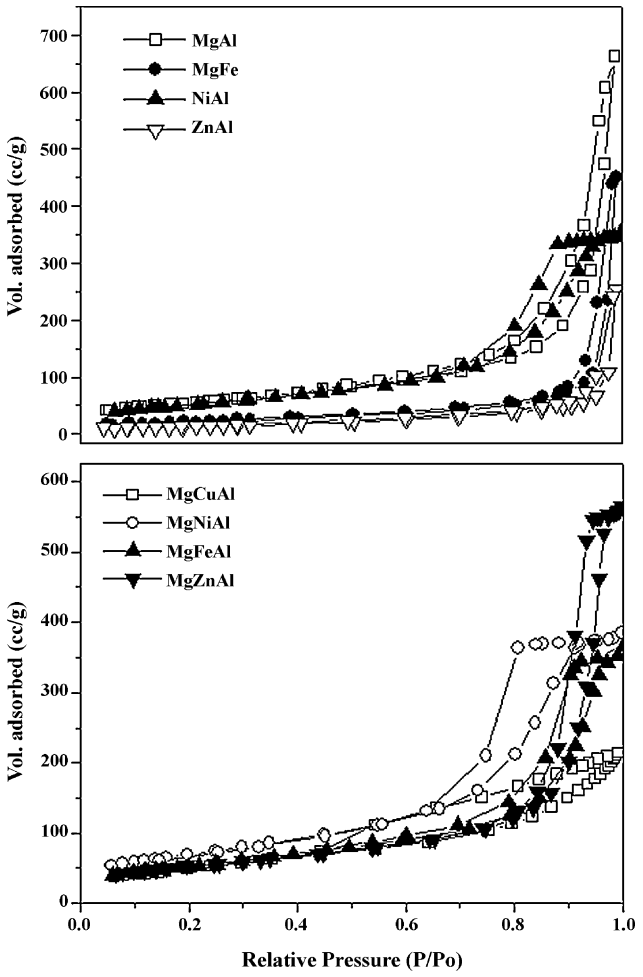

Fig. 2. Nitrogen adsorption–desorption isotherms of the samples calcined at 700 °C.

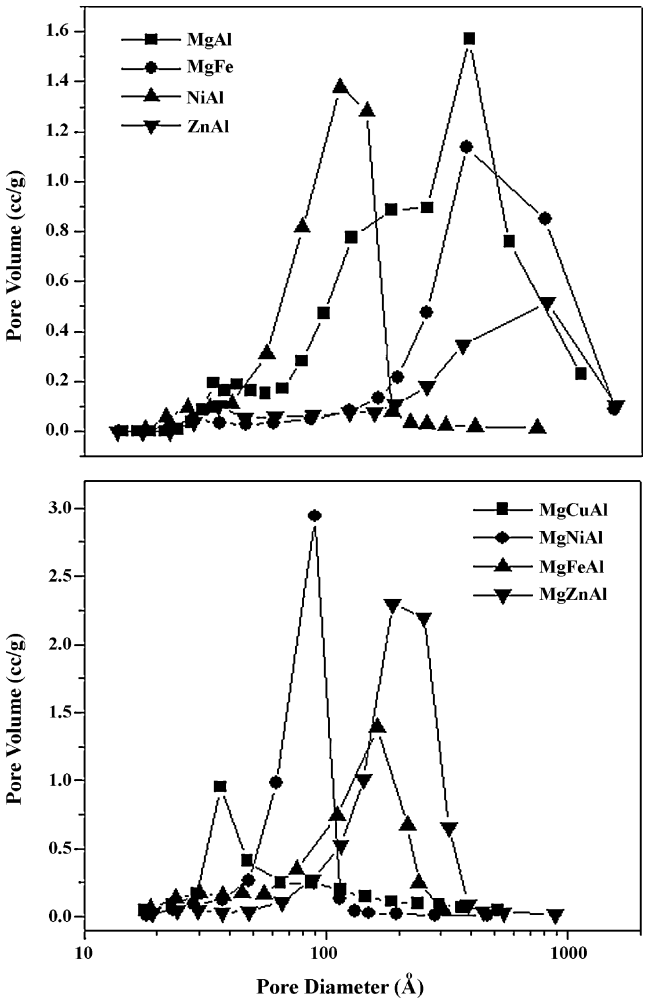

Fig. 3. Pore size distribution of the samples calcined at 700 °C.

respectively; while for the trimetallic compounds the values oscillated from 169 to 251 m^2/g. The pore volume in the bimetallic samples decreased in the following order MgAl > MgFe > NiAl > ZnAl while in the trimetallic ones it was MgZnAl > MgNiAl > MgFeAl > MgCuAl. The pore diameters of all samples fell in the mesopore range.

Fig. 2 shows the N_2 adsorption isotherms of the bimetallic and trimetallic HTs calcined at 700 °C for 4 h. All samples exhibited type IV isotherms, which are characteristic of mesoporous materials [28]. No point B was observed in the samples, indicating that a multilayer is formed from the beginning of the adsorption process. Notice that while MgAl, MgFe and ZnAl presented H3-type hysteresis loops, NiAl showed a type H1. Trimetallic HTs also present distinct hysteresis loops: MgNiAl exhibits type H1; MgFeAl and MgZnAl show type H3; while MgCuAl has a type H4 hysteresis loop. It is known that hysteresis is associated with the filling and emptying of the mesopores by capillary condensation, and the shape of the hysteresis loop varies from one material to another. The adsorption process is intimately related to the solid's morphology, and consequently to the pore shape [29]. Type H1

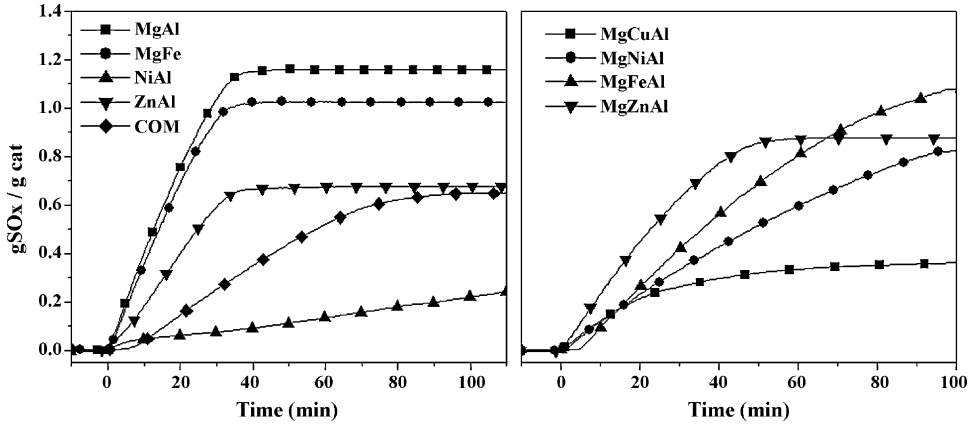

Fig. 4. SO_x adsorption isotherms of the first adsorption cycle.

Table 3
First SO_x adsorption cycle and total sulfated additive reduction percentages at 550, 650 and 700 °C.

Sample	Adsorption (g SO_x/g cat)			Saturation (g SO_x/g cat)	Time to reach saturation (min)	Sulfate species reduction (%)		
	5 min	10 min	15 min			550 °C	650 °C	700 °C
MgAl	0.20	0.40	0.59	1.15	50	9	57	100
MgFe	0.18	0.37	0.53	1.01	40	97	–	–
NiAl	0.03	0.05	0.06	0.30	145	100	–	–
ZnAl	0.08	0.19	0.30	0.67	65	43	96	–
MgCuAl	0.07	0.12	0.18	0.34	71	20	68	100
MgNiAl	0.06	0.12	0.18	0.82	98	41	97	–
MgFeAl	0.08	0.17	0.25	1.07	93	92	100	–
MgZnAl	0.04	0.16	0.27	0.87	67	29	95	–
COM	0.03	0.08	0.14	0.65	101	24	98	–

loops are given by adsorbents with a narrow distribution of uniform pores, while type H3 loops are found in materials made of aggregates of platy particles or adsorbents containing slit-shaped pores; type H4 hysteresis loops correspond to smaller slit-shaped pores [29]. Indeed, textural features of these solids can be explained in terms of the crystal size of the precursors HTs.

In calcined HTs, porosity is due to two different processes. Firstly, the smaller, intraparticle porosity is due to a "cratering" process that occurs during calcination [30]. Secondly, the plate-like particles collapse upon calcination in a disorderly manner, creating what has been described as a house-of-cards structure [31]. This interparticle porosity depends on the crystal size of the precursor HTs. Then, when small crystals such as those of NiAl and MgNiAl collapse, the stacking array is more ordered, and the resulting interparticle pores are smaller, more uniform, and with a narrow size distribution. This is reflected by the appearance of a type H1 hysteresis loop, and corroborated by the pore size distribution (Fig. 3). The same phenomenon occurs in MgCuAl, but the particles here are so small that a type H4 hysteresis loop appears. The pore size distribution is broad, but pores in the range of 20–80 Å account for a significant portion of the pore volume. On the other hand, when large crystals, such as those of MgAl, MgFe, ZnAl, MgFeAl and MgZnAl collapse, the result is a highly faulty stacking of particles, creating larger pores with a more heterogeneous distribution. These samples present H3 hysteresis loops and a very broad pore size distributions in the meso- and macropore range.

3.2. SO_2 adsorption–reduction test

Fig. 4 exhibits the SO_x adsorption isotherms of the first adsorption cycle. To compare solids from the industrial point of view, SO_2 adsorption was expressed as g SO_x/g cat. Results from Fig. 4 and Table 3 show that adsorption is highly influenced by the chemical composition, since the replacement of magnesium and/or aluminum by copper, iron, zinc or nickel resulted in a SO_2 pick-up capacity decrease, being: MgAl > MgFeAl ∼ MgFe > MgZnAl > MgNiAl > ZnAl > COM > MgCuAl > NiAl.

In addition to high adsorption capacity, SO_x additives used in the FCC process must also have high adsorption rates, to achieve suitable SO_x adsorption in short times. Therefore, SO_2 adsorption capacity was calculated at 5, 10 and 15 min, since the catalyst residence time in the regenerator falls in this range (see Table 3). Again, MgAl displayed the highest total SO_2 adsorption capacity with 0.20, 0.40 and 0.59 g SO_x/g cat at 5, 10 and 15 min, respectively, followed by MgFe, ZnAl, MgZnAl and MgFeAl. On the other hand, the nickel and copper-containing samples presented the lowest values in the 5–15 min interval.

It has been reported that SO_x adsorption rate can be improved by the incorporation of cerium oxide [2,18,32,33], but this compound is relatively expensive. In this case, its use was avoided by simply incorporating a transition metal in the hydrotalcite-like structure.

The catalytic behavior of the samples (except for the MgAl), cannot be assigned to their textural properties; it is better explained by their different redox abilities. For instance, MgFe and ZnAl samples having smaller surface areas (75 and 48 m^2/g, respectively), catalyze more easily the oxidation of SO_2 to SO_3 than NiAl (186 m^2/g). The only case where the SO_x pick-up can be explained in terms of basicity and surface area is that of the MgAl sample [32].

Although the adsorption rate and the total adsorption capacity are important parameters to compare solid's performance, other parameters such as reduction rate, reduction percentage, and the

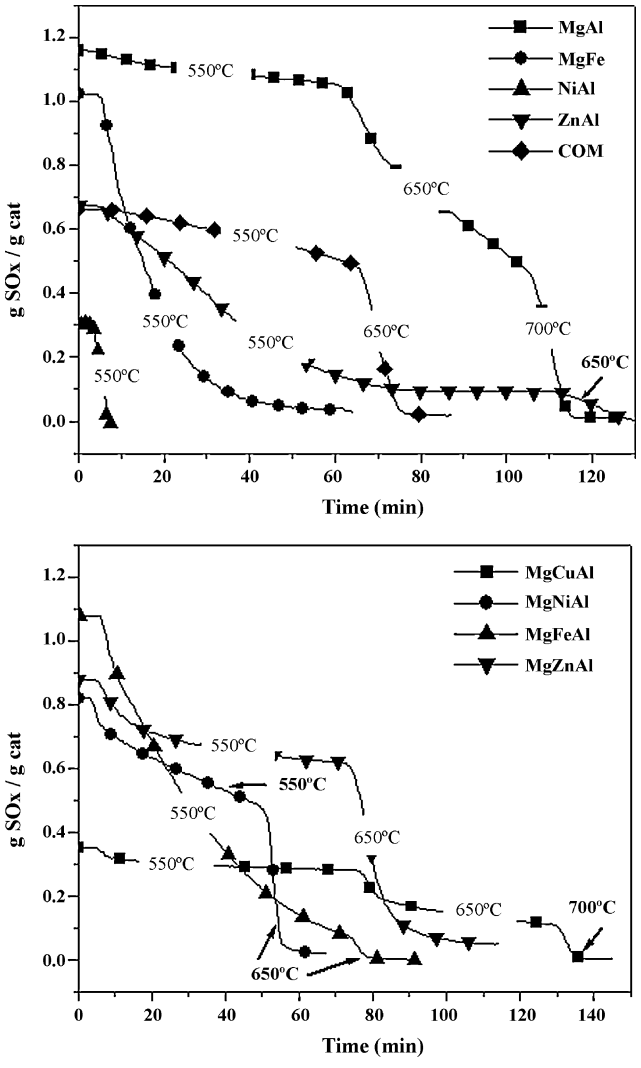

Fig. 5. Sulfated additives reduction profiles after saturation.

Table 4
Sulfated additive reduction percentages at 550, 650 and 700 °C determined at 1, 5 and 10 min.

Sample	Reduction percentage								
	550 °C			650 °C			700 °C		
	1 min	5 min	10 min	1 min	5 min	10 min	1 min	5 min	10 min
MgAl	0.15	1.38	2.81	0.19	3.79	15.64	2.44	25.81	81.10
MgFe	3.82	29.68	48.97	–	–	–	–	–	–
NiAl	14.52	100	–	–	–	–	–	–	–
ZnAl	0.29	6.24	13.96	0.88	18.68	49.45	–	–	–
MgCuAl	0.169	5.08	10.73	1.06	18.08	34.75	1.74	30.43	92.17
MgNiAl	1.93	12.62	17.73	5.91	87.97	94.04	–	–	–
MgFeAl	1.02	12.50	26.66	7.59	75.57	93.67	–	–	–
MgZnAl	0.34	6.73	14.25	.65	17.64	62.14	–	–	–
COM	0.45	1.82	3.94	1.00	18.00	71.00	–	–	–

catalyst regenerability are crucial for the lifetime of a given SO_x reducing additive. The reduction profiles presented in Fig. 5 illustrate the removal process of SO_x species adsorbed over the calcined hydrotalcite-like compounds after their saturation. Although the MgAl showed the highest SO_2 capacity, its sulfate reduction capacity is very limited, achieving only 9% at 550 °C and 57% at 650 °C, requiring increasing the temperature to 700 °C in order to eliminate all the adsorbed species (see last columns in Table 3). In this sense, Tagawa [34] studied the thermal decomposition of $Mg(SO)_4$ and $Al_2(SO_4)_3$ in flowing nitrogen and air and found that $Mg(SO)_4$ and $Al_2(SO_4)_3$ decompose at temperatures up to 800 and 493 °C, respectively. As Mg^{2+} and Al^{3+} are not reducible cations, the sulfate removal is mainly attributed to a thermal decomposition process.

When analyzing the other bimetallic samples, the incorporation of a transition metal instead of Mg^{2+} or Al^{3+} improved the elimination at 550 °C of the adsorbed species. The most remarkable were the MgFe (97%) and NiAl (100%) samples, while in the ZnAl and in the commercial sample (COM) the temperature had to be increased up to 650 °C in order to reduce the sulfate species, as is reported in Table 3.

Of the trimetallic compounds, only MgFeAl exhibited a suitable reduction percentage at 550 °C (92%), which is in good agreement with that reported previously [4,33,35]. On the other hand, although copper, nickel and zinc have redox characteristics to catalyze the regeneration, they are not effective. This may be due to the formation of stable sulfated species, which are then reduced to sulfides under reduction conditions [34]. These samples require higher temperatures (650 °C for MgZnAl and MgNiAl, 700° C for MgCuAl) in order to eliminate the adsorbed species, see Table 3.

Though the residence times in the riser are usually a few seconds [36], this time could be longer, depending on the FCC unit size and feed/catalyst flowing conditions. Tables 4 and 5 present SO_x reduction percentages and rates calculated at 1, 5 and 10 min at 550, 650 and 700 °C. First, the reduction rates and percentages were obtained at 1, 5 and 10 min at 550 °C. The remaining g SO_2/g cat adsorbed were then considered as the initial values for the calculations at 650 °C. The process is repeated at 700 °C, in order to compare reduction percentages and rates at these temperatures.

As can be appreciated in Table 4, the nickel and iron-containing samples exhibited the highest reduction percentages at 550 and 650 °C. NiAl was the most remarkable, eliminating the totality of the adsorbed species within 5 min. This effect was also reflected in the reduction rates reported in Table 5. For instance, at 550 °C, after 1 min, NiAl obtained a SO_x reduction rate of 4.36 g SO_x/min, followed by MgFe, MgNiAl and MgFeAl (1.88, 1.80, 1.07 g SO_x/min, respectively). After 5 min, reduction rates of the nickel-containing samples decreased, due to the fact that almost all of the adsorbed species were eliminated. While the low reduction rates of the MgCuAl at 550 °C remained nearly constant in the 1–10 min period, the iron and zinc-containing compounds increased their values, maintaining this behavior at 650 °C. It is clear that the sulfated species adsorbed by MgAl and MgCuAl are so strongly bound that they can only be totally eliminated at temperatures above 700 °C, achieving their highest reduction rates at this temperature (see Table 5).

After reduction, the solids were exposed to a second SO_2 adsorption cycle (see Fig. 6 and Table 6). MgAl, MgFe, MgNiAl, MgFeAl and COM showed similar adsorption capacities, demonstrating their regenerability. However, NiAl, ZnAl and MgZnAl showed a decrease in adsorption capacity, which may be explained by the formation of stable sulfides after the reduction step, exemplified by the following reactions:

$$3NiSO_4 + 10H_2 \rightarrow Ni_3S_2 + SO_2 + 10H_2O$$

$$2ZnSO_4 + 5H_2 \rightarrow ZnO + ZnS + SO_2 + 5H_2O$$

Sulfides poison the active sites for SO_2 adsorption. The inverse case is that of the MgCuAl sample, since the adsorption capacity was increased after reduction. MgCuAl showed, in the first adsorption cycle, an SO_2 adsorption capacity of 0.34 g SO_x/g cat, while in the second one it presented an increment of 65% (0.56 g SO_x/g cat). This behavior has been observed by other

Table 5
Sulfated additives reduction rates achieved at 550, 650 and 700 °C.

Sample	Sulfate species reduction rate ($\times 10^{-2}$ g SO_2 min^{-1})								
	550 °C			650 °C			700 °C		
	1 min	5 min	10 min	1 min	5 min	10 min	1 min	5 min	10 min
MgAl	0.03	0.34	0.32	0.21	1.9	2.40	1.07	5.65	4.90
MgFe	1.88	6.89	3.76	–	–	–	–	–	–
NiAl	4.36	1.78	–	–	–	–	–	–	–
ZnAl	0.06	0.62	0.97	0.05	0.45	0.57	–	–	–
MgCuAl	0.11	0.68	0.12	0.27	1.58	0.42	0.16	1.81	0.42
MgNiAl	1.80	0.67	0.45	1.10	10.10	0.22	–	–	–
MgFeAl	1.07	3.88	2.00	0.53	1.47	0.15	–	–	–
MgZnAl	0.04	1.85	1.01	0.15	2.80	5.34	–	–	–
COM	0.08	0.26	0.24	0.52	4.73	4.49	–	–	–

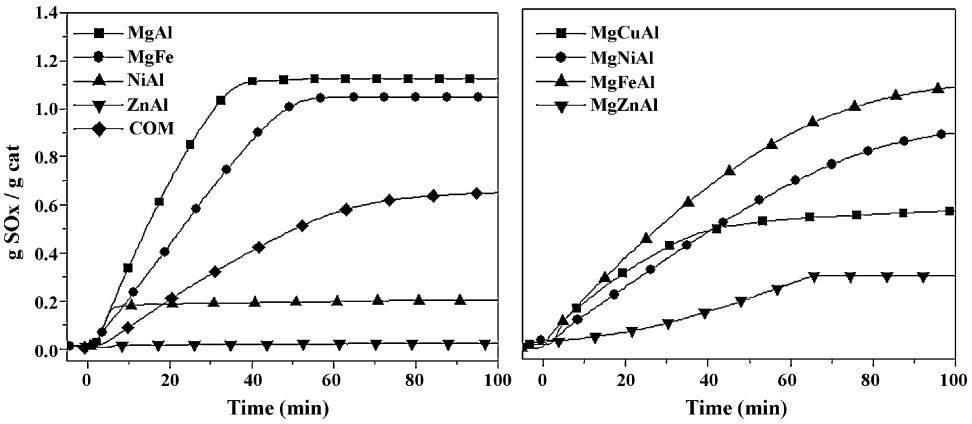

Fig. 6. SO_x adsorption isotherms of the second adsorption cycle.

Table 6
Second SO_x adsorption cycle.

Sample	Adsorption (g SO_x/g cat)			Saturation (g SO_x/g cat)	Time to reach saturation (min)
	5 min	10 min	15 min		
MgAl	0.19	0.39	0.57	1.11	50
MgFe	0.12	0.23	0.34	1.04	54
NiAl	0.16	0.18	0.18	0.19	77
ZnAl	–	0.01	0.02	0.02	46
MgCuAl	0.13	0.20	0.27	0.56	105
MgNiAl	0.09	0.15	0.19	0.85	101
MgFeAl	0.13	0.22	0.30	1.08	104
MgZnAl	0.02	0.03	0.04	0.29	76
COM	0.04	0.09	0.15	0.66	118

(–) Not observed.

authors in MgCuAl hydrotalcites, where they explained that, during reduction, Cu^0 is formed, and in the second adsorption cycle the reduced copper species consume oxygen to form CuO, which is also active for catalyzing the oxidation of SO_2 to SO_3 [32].

4. Conclusions

Bimetallic and trimetallic hydrotalcite-like compounds were synthesized by coprecipitation. The obtaining of pure HT structure was corroborated by XRD analysis. Calcined HTs were tested as SO_x removal catalysts. The SO_2 pick-up efficiency of the samples was MgAl > MgFeAl ∼ MgFe > MgZnAl > MgNiAl > ZnAl > COM > MgCuAl > NiAl. By introducing a transition metal inside the layers of the hydrotalcite-like structure, the adsorption capacity increased, being the most remarkable in the bimetallic and trimetallic iron and zinc-containing samples.

The effect of the transition metal was also important in the reduction process, since all the adsorbed species were reduced at 550 or 650 °C (except for the MgAl and MgCuAl). Finally, when the calcined compounds were evaluated in a second SO_2 adsorption cycle MgAl, MgFe, MgNiAl, MgFeAl and COM showed similar values than those found in the first cycle, while NiAl, ZnAl and MgZnAl showed a marked decrease attributed to the formation of stable sulfides, which poisons the active sites for SO_x adsorption.

Considering the conditions found in the FCC regenerator-riser zones, the results here presented suggest that the iron-containing hydrotalcite-like compounds could be considered as potential SO_2 reducing materials for the FCC process.

Acknowledgement

Authors thank the Instituto Mexicano del Petroleo for the financial support.

References

[1] Sulfur oxides emissions from fluid catalytic cracking unit regenerators – Background information for proposed standards; Report EPA-450/3-82-013a. U.S. Environmental Protection Agency, Research Triangle Park, NC, 1984.
[2] A.A. Bhattacharyya, G.M. Woltermann, J.S. Yoo, J.A. Karch, W.E. Cormier, Ind. Eng. Chem. Res. 27 (1988) 1356.
[3] T.J. Pinnavaia, J. Amarasekera, C.A. Polansky, US Patent 5 114 691 (1992).
[4] T.J. Pinnavaia, J. Amarasekera, C.A. Polansky, US Patent 5 114 898 (1992).
[5] D. Bienstock, J.H. Fiel, US Patent 2 992 884 (1961).
[6] F.W. Pijpers, M.M.J.J. Starmans, US Patent 3 411 865 (1968).
[7] J.S. Yoo, A.A. Bhattacharyya, C.A. Radlowski, Ind. Eng. Chem. Res. 30 (1991) 1444.
[8] R.J. Bertolacini, E.H. Hirschberg, F.S. Modica, US Patent 4 497 902 (1985).
[9] J.S. Yoo, A.A. Bhattacharyya, C.A. Radlowski, J.A. Karch, Appl. Catal. B 1 (1992) 169.
[10] J.S. Yoo, C.A. Radlowski, US Patent 4 492 678 (1985).
[11] J. Mooi, US Patent 4 472 532 (1984).
[12] M. O'Conell, M.A. Morris, Catal. Today 59 (2000) 387.
[13] A. Trovarelli, C. Leitenburg, M. Boaro, G. Dolcetti, Catal. Today 50 (1999) 353–367.
[14] J. Wang, L. Chen, C. Li, J. Mol. Catal. A 139 (1999) 315.
[15] T. Zhu, A. Dreher, M. Flytzani-Stephanopoulos, Appl. Catal. B 21 (1999) 103.
[16] R.M. Ferrizz, R.J. Gorte, J.M. Vohs, Catal. Lett. 82 (1–2) (2002) 123.
[17] M. Waquif, A.M. Saad, M. Bensitel, J. Bachelier, O. Saur, J.-C. Lavalley, J. Chem. Soc. Faraday Trans. 88 (19) (1992) 2931.
[18] J.S. Yoo, A.A. Bhattacharyya, C.A. Radlowski, J.A. Karch, Ind. Eng. Chem. Res. 31 (1992) 1252.
[19] A.A. Vierheilig, US Patent 2003/0203806 A1 (2003).
[20] A. Corma, A.E. Palomares, F. Rey, F. Márquez, J. Catal. 170 (1997) 140.
[21] A.E. Palomares, J.M. López-Nieto, F.J. Lázaro, A. López, A. Corma, Appl. Catal. B 20 (1999) 257.
[22] J. Valente, F. Figueras, M. Gravelle, P. Khumbar, J. López, J.-P. Besse, J. Catal. 189 (2000) 370.
[23] F. Cavani, F. Trifirò, A. Vaccari, Catal. Today 11 (1991) 173.
[24] M.C. Gastuche, G. Brown, M.M. Mortland, Clay Miner. 7 (1967) 177.
[25] L.V. Azároff, M.J. Buerger, The Powder Method in X-ray Crystallography, McGraw-Hill, New York, 1958.
[26] G. Brown, M.C. Gastuche, Clay Miner. 7 (1967) 193.
[27] G.W. Brindley, S. Kikkawa, Am. Miner. 64 (1979) 836.
[28] S.J. Gregg, K.S.W. Sing, Adsorption, Surface Area and Porosity, Academic Press, 1982.
[29] F. Rouquerol, J. Rouquerol, K. Sing, Adsorption by Powders and Porous Solids. Principles, Methodology and Applications, Academic Press, London, 1999.
[30] W.T. Reichle, S.Y. Kang, D.S. Everhardt, J. Catal. 101 (1986) 352.

[31] J.A. Gursky, S.D. Blough, C. Luna, C. Gomez, A.N. Luevano, E.A. Gardner, J. Am. Chem. Soc. 128 (2006) 8376.
[32] A. Corma, A.E. Palomares, F. Rey, Appl. Catal. B 4 (1994) 29.
[33] M. Cantu, E. Lopez-Salinas, J.S. Valente, R. Montiel, Environ. Sci. Technol. 39 (2005) 9715.
[34] H. Tagawa, Thermochim. Acta 80 (1984) 23.
[35] J. Wang, L. Chen, C. Li, React. Kinet. Catal. Lett. 64 (1998) 73.
[36] R. Sadeghbeigi, Fluid Catalytic Cracking Handbook. Design, Operation and Troubleshooting of FCC Facilities, 2nd edition, Gulf Publishing Company, 2000.